INFLUENCE OF A HELICOPTER TAIL ROTOR SHROUD ON THE INTERACTION NOISE DUE TO THE MAIN ROTOR VORTICES

M. Weisgerber, G. Neuwerth
Institut für Luft- und Raumfahrt der RWTH-Aachen
52062 Aachen, Germany

Abstract

In this paper the topic of **B**lade-**V**ortex-**I**nteraction (BVI) of the main rotor blade tip vortices with the helicopter tail rotor will be presented. Special interest is addressed to the influence of a shroud around the tail rotor on this interaction. For this purpose an experimental setup was built using a 1:1.43 scale model of a Fenestron tail rotor of an EC-135 helicopter with the capability of removing the shroud. It was used in a wind tunnel for noise and flow field measurements. Some clear differences in the spectra and flow fields were seen. Though for the cases with and without shroud, the increase in noise pressure with vortex interaction was nearly identical, the differences in the spectra were significantly. The standard tail rotor gained a lot of extra tones, separated by the vortex-passing-frequency while the Fenestron only gained in its already existing frequencies. So the perceived noise changes were more unfortunate for the standard tail rotor becoming more *metallic* in quality.
Furthermore a theoretical examination of the BVI was done using the formalism of Lighthill and Ffowcs-Williams/Hawkings. In combination with blade element theory a computer program was written, which calculates the noise emissions of the tail rotor on a semi empirical basis. It uses the measured flow fields as input for the calculation of the pressure distributions and fluctuations whereby the vortex was superposed by a model. The overall noise pressure levels are shifted compared to the experiments but the increase due to vortex interactions is the same as in experiments. Some problems still exist regarding the spectrum of the calculated noise with some frequencies too high, wile others are missing. A solution may be using a smaller time separation of the iteration steps, or using a more complex theoretical approach.

Used Variables

$\alpha_{i(r)}$	effective angle of attack of rotor blade at radial position r
$\alpha_{\text{Fenestron}}$	geometric angle of attack of rotor blade at blade tip
$\alpha_{\text{VortexGenerator}}$	geometric angle of attack of vortex generator blade at blade tip
$\phi_{(r)}$	geometric angle of attack for blade at radial position r
ρ	density of air
Γ	circulation of vortex
A_α	absorption area of reverberation room
a_0	speed of sound in air
$f_{\text{Tailrotor}}$	blade passing frequency of tail rotor
f_{Vortex}	passing frequency of vortex trail
F_i	i-component of noise dipole term
K_0	noise pressure level correction based on temperature fluctuations
K_{01}	noise pressure level correction based on measured frequency band ”Waterhouse Term”
L	noise pressure level
L_{m}	measured noise pressure level
p, p_i, p_{ij}	pressure components respectively
Q	noise mono pol term
q	dynamic pressure
r	radius component
R_c	core radius of vortex
t	time

T_{ij}	Lighthill stress tensor
T_{echo}	echo time of reverberation room
T_{xxx}	period of subscript
V	volume
$\Delta v_{(r)}$	velocity increase at rotor disc
v_{inflow}	velocity of rotor inflow
$v_{\mathrm{tan\,vortex}}$	tangential velocity component of vortex
v_{n}	normal component of velocity
v_z	velocity component in z direction at core radius

Introduction

In modern times, helicopters are an often used and important air transportation vehicle. Due to its special flight capabilities it is an extraordinate tool for modern civilian life tasks, e.g. emergency transportation of sick people, organ transplants, or traffic monitoring, etc.
But those flight missions mostly take place in densely populated regions of cities. Within these environments, noise is of high importance, because due to everyday life noise levels already gain heights of about 90 dB(A) over daytime while the German Ministry of Health advises a mean threshold value for the exposure to noise of 65 dB(A) for daytime and 55 dB(A) for nighttime.
The best known noise sources of helicopters are of course the main rotor and the engines. Older models, e.g. Bell UH-1, with just two very long main rotor blades are associated with typical helicopter noise, known as “flapp-flapp”, originating from locally distributed supersonic air flow on the blades. These were easily reduced by using more and shorter blades, up to five can be seen at the newest helicopters of Eurocopter. In so doing the tangential velocity of the blade tips and the load on the blades were decreased. Both lead to lower noise emissions. Further on, usage of modern turbines and improvements on the exhaust systems resulted in more silent helicopters.
By reducing these two noise emitters, the tail rotor gains importance. Already in the 1970‘s Leverton [1] showed that the tail rotor noise can be the dominant noise source in special flight conditions exceeding the noise pressure level of the main rotor by more than 15 dB. He also made measurements on the influence of the so called Blade-Vortex-Interaction (BVI) noise. This occurs mainly in low speed flight situations

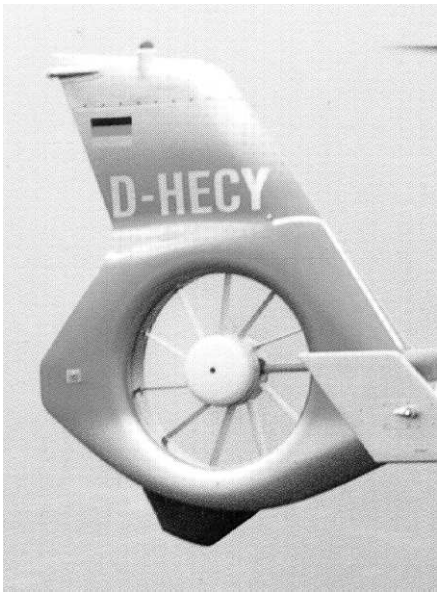

Figure 1: Fan-in-fin integration of a helicopter tail rotor, “Fenestron”

with climbing or descending, i.e. during take-off or landing. During these the tip vortices shed from the main rotor can interact with the rotating tail rotor blades with the vortex axis perpendicular to the tail rotor plain. This interaction produces periodically changing flow patterns on the tail rotor blades, resulting in differential force changes. In this way pressure fluctuations are induced which spread out into space and are perceived as an increase in noise.
The topic of vortex interaction noise with tail rotors is widened by the fact, that there are different implementation of tail rotors:

- free tail rotors, rotating alongside the tail fin and
- fan-in-fin integrations, so called *Fenestron*, with the rotor rotating inside a duct as is shown in figure 1.

Not only has the Fenestron advantages in operations and thrust parameters but the shroud also has an dramatic effect on the noise emitted as can easily be seen in figures 2 and 3. They show the spectra of the two tail rotor types for forward flight at 17 m/s. There the free rotor exhibits a broader spectrum with the maxima at the blade passing frequency and its corresponding harmonics. In contrast the Fenestron engenders a very tonal spectrum of eye-catching maxima, with intermediate frequen-

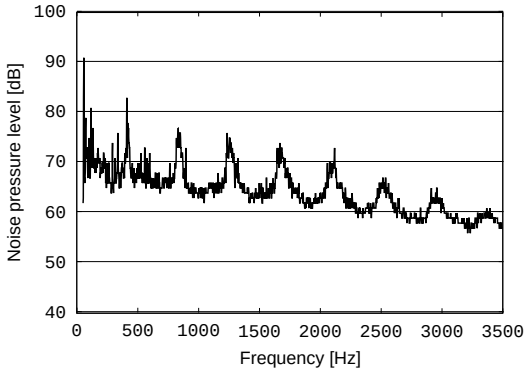

Figure 2: Spectrum of the standard tail rotor

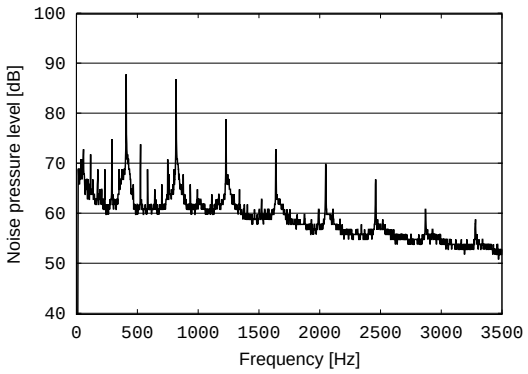

Figure 3: Spectrum of the Fenestron

cies of no relevance between the harmonics. There will naturally be an effect on the blade vortex interaction due to the shrouding. The examination of this effect constitutes the topic of this investigation.

So far most work on the blade vortex interaction noise was done on systems having the axis of the interacting vortex parallel to the rotation plane of the rotor, as is reported by Caradonna et. al. [2], Kitaplioglu et. al [3] or Srinivasan et. al. [4]. But in this case the blade tip vortices of a helicopter main rotor will interact at right angles with the tail rotor plane. To adhere to this behaviour a special test bench was constructed, which will be explained in the next section.

Experimental setup

For the measurements of the noise spectra and the flow field around the Fenestron, a 1:1.43 scale model of a Fenestron, as used for the EC-135 helicopter, was used. The rotor consists of 7 blades and has a diameter of 0.7 m. This model was placed in the free test section of the subsonic wind tunnel of the **I**nstitut für **L**uft- und **R**aumfahrt (ILR); a sketch of it is shown in figure 4.This test section is 3 meters in length and the maximum useful diameter of airflow at the nozzle is 1.5 meters.

As can be seen in figures 5 and 6 the model of the Fenestron is situated near the middle of the test section. Upstream, directly in front of the nozzle outlet a propeller is placed as vortex generator. In figure 5 the used coordinate system is shown. The vertical position is chosen in such a way, that only the bottom part of the vortex trail will interact orthogonal with the tail rotor. The vortex generator is driven by the engine of the Fenestron using tooth belts. Using this power transmission has the advantage, that the relative phase of vortex generator and Fenestron stays fixed and can be restored easily when the experiment is setup the next time. Otherwise the reproducibility would not be assured. Also the fitting of the vortex generator

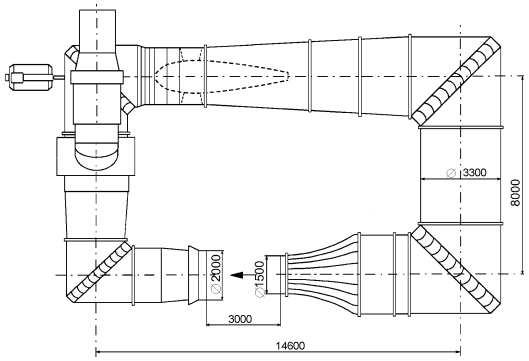

Figure 4: Sketch of the subsonic wind tunnel of the Institute of Aerospace Engineering of the RWTH-Aachen

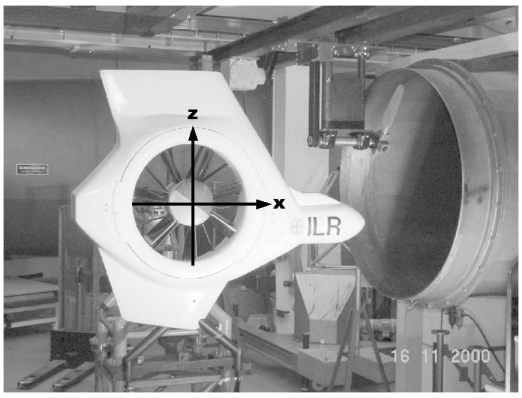

Figure 5: Experimental setup of the Fenestron and the vortex generator

and the belt system had to be considered very carefully, otherwise the flow pattern would be distorted too much. The belt mostly of its way

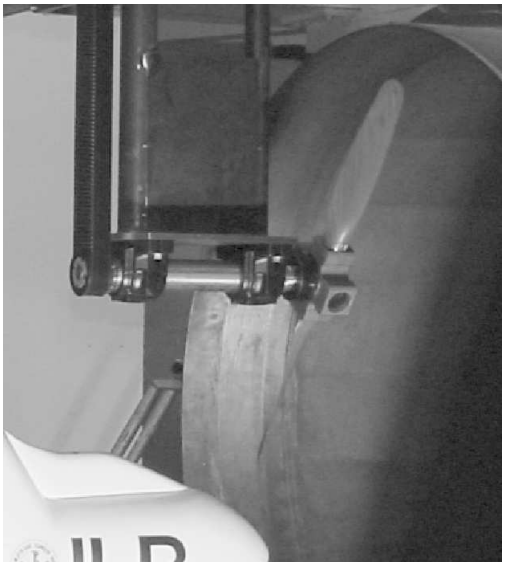

Figure 6: Detail window of vortex generator and belt system

runs outside the wind tunnel stream, and is hidden behind an aerodynamically shaped fitting during its decline towards the vortex generator axis, as can be seen in figure 6. By using different lock washers, nearly any gear ratio can be used. Preliminary test showed the biggest effect of the vortex interaction for an experimental setup using the parameters as shown in table 1.

Table 1: Standard parameters of experimental setup

Fenestron RPM	3500 1/min
Gear ratio	5/7
$\Rightarrow$ Vortex Generator RPM	2500 1/min
$\alpha_{\text{Fenestron}}$	$25°$
$\alpha_{\text{Vortex Generator}}$	$20°$
Velocity of wind tunnel	17 m/s

The typical vortex and rotor related constants, like vortex circulation Γ, diameter of the vortex core and the passing frequencies of the vortices and the tail rotor blades for these parameters are given in table 2.
As will be seen later, for a reliable analysis of the flow field measurements, the vortex passing frequency and the tail rotor blade passing frequency are of special interest.

Table 2: Vortex and tail rotor related values

Γ	1.8 m^2/s
$v_{\text{tan Vortex}}$	20 m/s
R_c	0.014 m
f_{Vortex}	83 Hz
$f_{\text{Tailrotor}}$	409 Hz

Because the wind tunnel room holds the features of a reverberation chamber, as shown by Schreier [5], it can be used for noise measurements. But some corrections terms [6] have to be added to the measured noise level L_{m} as given in equation 1.

$$L = L_{\text{m}} + \left[10 \cdot \log_{10} \left(\frac{A_\alpha}{1\,m^2} \right) - \right. \\ \left. -6 + K_0 + K_{01} \right] \tag{1}$$

K_0 and K_{01} are correction terms regarding temperature and frequency dependent influences and A_α being the absorption area of the room. The latter can be calculated by the so called Sabine-Equation given, in equation 2

$$A_\alpha = 0.135 \cdot \frac{V}{T_{\text{echo}}} \tag{2}$$

when the volume of the room V and the echo-time T_{echo} are known. T_{echo} is the time needed for a broadband signal to decay to less than 10^{-6} of the starting signal after being switched off.
Because the Fenestron noise signals have a tonal character, these signals will form standing waves inside the room. To avoid measurements in a wave knot, during the noise measurements the microphone is moved along a circle of 3 meters in radius. The centre point of the circle is 11 meters away from the Fenestron.

Experimental results

First the results of the noise measurements will be presented, followed by the flow field examinations.

Noise

As was shown in figure 3 the Fenestron has a very tonal spectrum with the strongest signal at the fundamental or blade passing frequency, here at 409 Hz. The overall noise pressure level

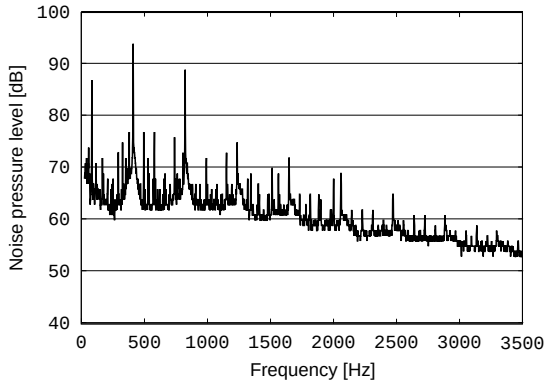

Figure 7: Spectrum of the Fenestron with BVI

as shown in figure 3 has a value of 97 dB. With the blade vortex interaction there is an increase in the overall noise level as can be seen in figure 7. The increase has the magnitude of 4 dB. There are also some intermediate peaks visible. Their separation equals the vortex passing frequency, i.e. 83 Hz. This proves that they are directly related to the existence of the vortices. But their magnitude is not high enough to have a big effect on noise level and noise quality.
The spectrum for the standard tail rotor with BVI is very different, as shown in figure 8. The levels of the tail rotor fundamental frequency and harmonics are nearly unchanged. Accessorily, there are many strong signals between the rotor frequencies. Again their frequency separation equals the vortex passing frequency. So

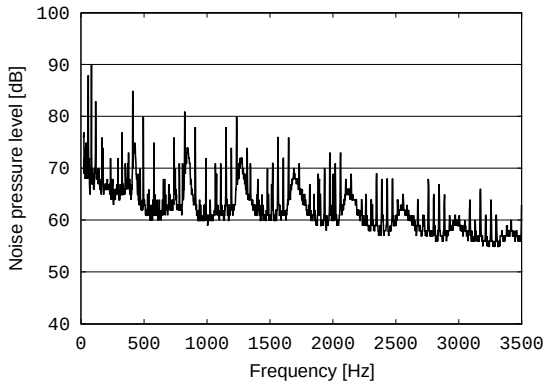

Figure 8: Spectrum due to BVI of the standard tail rotor

they are also directly connected to the vortices. Here their number and levels are high enough to have an effect on the overall noise level and the noise quality. The total increase of noise is again about 4 dB from 98 dB (without BVI) to 103 dB (with BVI), but more important is the change of the perceived noise quality. The standard tail rotor with the spectrum of figure 8 has a very $metallic$ character which is far more annoying to hear than an increased single tone. The results of the acoustic measurements are summarised in table 3. Because the free rotor gains a lot of signals in the frequency band between 1000 and 3000 Hz the application of the A-weighting is interesting to include the natural sensitivity of the human ear. The standard tail rotor is about 3 dB(A) lower in his noise emissions than the Fenestron when no BVI occurs. This changes, when the vortex interaction is included. With BVI the free rotor is about 2.5 dB(A) louder than the Fenestron. The A-weighted results are also given in table 3.

Table 3: Summary of measured noise levels

	Fenestron	Std.Tail Rotor
without BVI	97.5 dB	98.2 dB
with BVI	101.2 dB	103.4 dB
without BVI	95.6 dB(A)	92.6 dB(A)
with BVI	103.1 dB(A)	105.7 dB(A)

Flow fields

The explanation for the significant differences in the spectra has to be found in the flow fields involved. Figure 9 shows a measurement of the flow field including the vortex, at about 10 cm in front of the Fenestron inlet surface and 40 cm upstream of the Fenestron axis, such that the

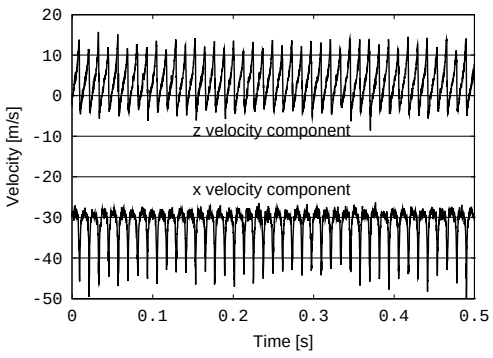

Figure 9: Hot wire anemometry time signal with vortex influence

rotor influence can be neglected. Shown are the x- and z-components respectively. This time signal shows clearly the superposition of the vortex induced velocity with the wind tunnel velocity. Now the examination of the flow field is twofold:

1. By performing a **F**ast-**F**ourier-**T**ransformation (FFT) on the time signal, one gets a correlation of the vortex strength by means of the amplitude of the corresponding FTT-frequency. The same approach is useful for the blade passing frequency of the tail rotor itself. Here the influence of the tail rotor on it's surroundings can be determined, which also has an influence on the BVI.

2. Calculating a mean-vortex by superposing the measured vortices, gives the mean induced velocity for the three space variables. Here the influence of the shroud on the vortex structure can be examined.

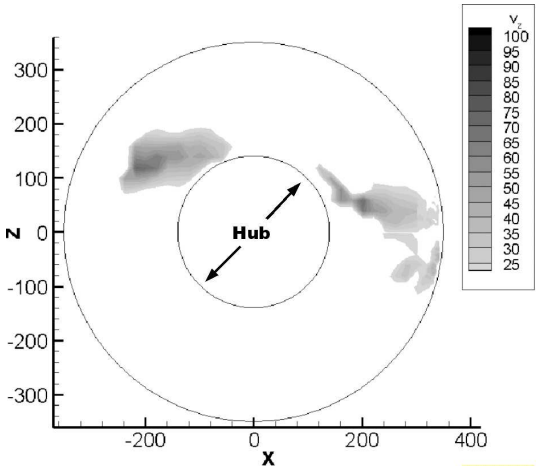

Figure 10: Amplitude of Fourier transform for v_z of vortex frequency 83 Hz in Fenestron inflow

In figures 10 and 11 the standardised amplitudes for the Fenestron and standard tail rotor are shown respectively. The view is head on to the rotor disc with the wind tunnel stream and the vortices flowing in from the right. The outer circle represents the rim of the rotor disk and the inner the rotor hub.
Clear differences in the amplitude strengths and distributions are visible. First, the amplitudes for the standard tail rotor are much higher than for the Fenestron. Because the values of the amplitudes depend on the values of

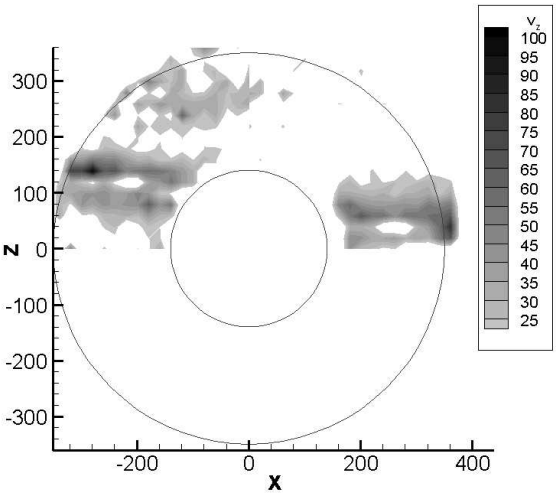

Figure 11: Amplitude of Fourier transform of vortex frequency (83 Hz) for v_z in standard rotor inflow

the vortex induced velocities the latter are also higher for the free rotor than for the Fenestron. Also the primary interaction point is more downstream in the case of the Fenestron. This is the consequence from the turbulent inflow which originates in the upstream directed portion of the Fenestron ring. Vortices can move along these boundary layers just as on solid surfaces. In contrast, the vortex tube encounters the rotor blades directly at the blade radius in case of the standard tail rotor. Therefore, in figure 11 a strong interaction point can be seen just on the rim of the tail rotor area. An analogous situation is found for the most downstream interaction area. Again in case of the standard tail rotor the interaction is more on the rim and stronger than in the case of the Fenestron.
Also, the strength of the vortex induced velocities are greater and the interaction points are more to the outside of the rotor plane.
Herein we find the reasons for the differences in the spectra. Because the generation of noise mainly takes place within the outer 20 to 25% of the rotor disc, the stronger interaction of the vortices with the tail rotor within this radial position results in stronger emissions with frequencies related to the vortex passing frequency. The signals within the higher frequency domain of the spectrum are then the combination of the rotor harmonics with the vortex frequency harmonics. In contrast the interaction point with the Fenestron blades is more towards the axis, in regions less important for noise generation.

So only the total velocity increase of the inflow has effects on the increase of noise pressure.

Theoretical background of noise calculations

The demand on the theoretical examinations was the development of a quick and robust system for calculations. The use of Euler- or even Navier-Stokes-Theorems were not practical due to time restrictions. So the approach of combining momentum- and blade-element-theories was tried. As Adkins et. al. [7] shows the blade-element-theory gives quite good results. By using the mean measured velocity fields as near to the tail rotor blades as possible and combining them with the momentum theory and thrust measurements, one can find the effective angle of attack on the tail rotor blades. With these at hand one can easily calculate the velocity and pressure distributions on the different blade elements of the rotor blades. For the calculation of the effective angle of attack $\alpha_{i(r)}$ equation 3 given by Schlichting [8] was used:

$$\alpha_{i(r)} = \tan^{-1}\left(\frac{\Delta v_{(r)}}{v_{\text{inflow}(r)} \cdot \cos\left(\phi_{(r)}\right)}\right) \qquad (3)$$

with $\Delta v_{(r)}$ being the velocity increase at the rotor disc, v_{inflow} is the inflow velocity and $\phi_{(r)}$ is the geometric angle of attack in dependence of the radial position along the blade.
With this effective angle of attack and the dynamic pressure of the inflow

$$q = \frac{\rho_\infty}{2} v^2_{inflow} \qquad (4)$$

the lift and friction forces can be calculated. Combining these gives the thrust which is already known by measurements and the stream theory. Now, one can calculate backwards, to find the velocity and pressure distributions on the panels the rotor blades are made of.
For BVI simulation a vortex model, like the Rankine (see equation 5) is superimposed on the measured stationary rotor inflow:

$$v_r = 0\ ,\ v_t = \frac{\Gamma}{2\pi} \cdot \begin{cases} \frac{r}{R_c^2} & r < R_c \\ \frac{R_c^2}{r} & r > R_c \end{cases} \qquad (5)$$

where v_r is the radial velocity component and v_t the tangential velocity component of the vortex. r stands for the radial distance from the vortex centre and R_c is the vortex core radius. As seen in the previous section on the analysis of the inflow fields, the foot point of the vortex spirals moves along a stable path over the front side of the tail rotor plane. This and the change in circulation and axis orientation is accounted for by the use of spline functions over selected points giving the values needed for calculating the vortex induced velocities as a function of the position on the rotor plane. Studies for different vortex parameters can then easily be accomplished by changing the sampling points used by the spline functions.
Afterwards, the emitted noise is calculated using the formalism of Lighthill [9] and Ffowcs-Williams/Hawkings [10].
As Lighthill showed with his acoustic analogy and application of the Lighthill stress tensor T_{ij}

$$T_{ij} = \rho v_i v_j + p_{ij} - a_0^2 \rho \delta_{ij} \qquad (6)$$

with density ρ, velocity components v_i, v_j, speed of noise a_0 and Kronecker delta δ_{ij}, the inhomogeneous wave equation for noise can be given as shown in equation 7

$$\frac{1}{a_0^2}\frac{\partial^2 p}{\partial t^2} - \frac{\partial^2 p}{\partial x_j^2} = \frac{\partial Q}{\partial t} - \frac{\partial F_i}{\partial x_i} + \frac{\partial^2 T_{ij}}{\partial x_i \partial x_j} \qquad (7)$$

with the following terms on the right hand side:

$$\text{Monopole term} \quad \frac{\partial Q}{\partial t} \qquad (8)$$

$$\text{Dipole term} \quad \frac{\partial F_i}{\partial x_i} \qquad (9)$$

$$\text{Quadrupole term} \quad \frac{\partial^2 T_{ij}}{\partial x_i \partial x_j} \qquad (10)$$

Equation 8 describes the noise emission due to the air displacement by the blade, equation 9 considers the noise created by forces acting on the blade and equation 10 the noise from turbulent stresses. Because the velocities involved here are too small, the quadrupole part is neglected. On the other hand, the vortex influence will mostly be related to the dipole noise term because of the fluctuations of the forces acting on the blades due to flow variations.
The next step involves the extension made by Ffowcs-Williams and Hawkings. They considered the Lighthill equation 7 for solid boundaries in arbitrary motion. In the end the equation of Ffowcs-Williams/Hawkings has the form

of equation 11, as can be found by Farrasat [11]

$$4\pi p_{(\vec{r},t)} = \frac{\partial}{\partial t}\int\left[\frac{\rho_0 v_\mathrm{n}}{r\cdot|1-M_r|}\right]_\mathrm{ret} dS + \\ + \frac{1}{a_0}\frac{\partial}{\partial t}\int\left[\frac{p_r}{r\cdot|1-M_r|}\right]_\mathrm{ret} dS \qquad (11)$$

where v_n is the normal component of the velocity on the rotor blade surface, p_r is the pressure component of the blade panel in the direction of the observer and M_r being the Mach number. The index "ret" means that the calculation has to be done at the retarded time, when the pressure fluctuation received by the observer is produced at the regarded panel.
This calculation is performed for all seven blades separately and subsequently superposed phase correct. The calculation is done for one sub period. This means, that the real periodicity of the vortex-rotor-system would be the time needed for the rotor having its blades reorientated as in the starting position and the vortex distribution like at the beginning of the calculation. This situation is reached at the smallest common factor of the respective periods

$$T_\mathrm{vortex} = 0.012\,s\ ,\ T_\mathrm{blade} = 0.017\,s \\ \Rightarrow\ T_\mathrm{common} = 0.204\,s \qquad (12)$$

Using a time step of $0.000048\,s$ this would lead to 4250 rounds of calculation; about 17 days of computing. If one ignores the order of the rotor blades, and instead only demands, that any one blade has a horizontal upstream orientation and the vortex distribution is the same as at the beginning, this would be a sub period. Appending them to one another will also lead to a full period of T_common. One sub period has a length of $0.0024\,s$, so after just 250 time steps the sub period is done. This is a 1/17$^{\mathrm{th}}$ of the prior calculation time.

Results of theoretical calculations

In figure 12 the calculated noise pressure levels for the Fenestron with and without vortex interaction are shown. In the figure the azimuthal angle starts to the horizontal right at $0°$ and sweeps counter clockwise. With this convention the Fenestron plane is aligned vertical and the wind tunnel airflow comes from $90°$. This predefinition also holds true for figure 13 showing the results for the standard tail rotor.

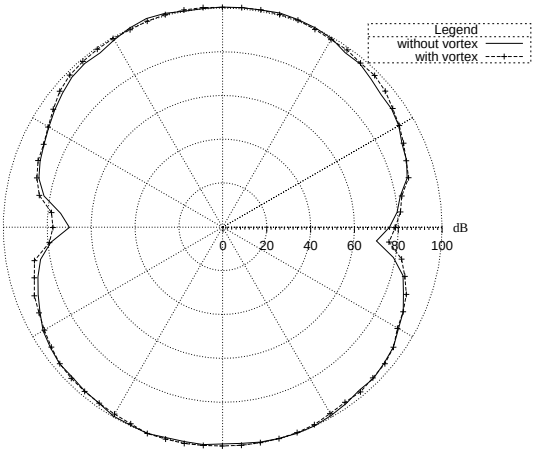

Figure 12: Angular distribution of calculated noise pressure levels for the Fenestron with and without vortex interaction

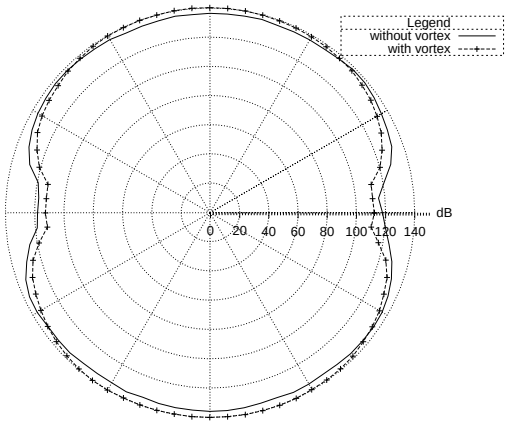

Figure 13: Angular distribution of calculated noise pressure levels for the standard tail rotor with and without vortex interaction

The calculations and experiments were performed for the same parameters, i.e. 3500 RPM for the Fenestron and a vortex passing frequency of 83 Hz. The plots show the results for the horizontal plane of inclination angle $90°$. The dipole character of the radiation can be clearly seen. Also a slight increase in noise pressure level is cognisable. The asymmetric appearance follows from the asymmetric inflow because of the wind tunnel air speed, therefore the minima are not exactly opposed each other at azimuthal angels of $0°$ and $180°$.
The same is found for the standard tail rotor, except that here the overall pressure level shift is bigger in magnitude. But again the increase in noise pressure level due to the vortex interaction is about the same size as was measured.

A summary of the calculated values can be found in table 4. A comparison of these results

Table 4: Summary of calculated noise levels

	Fenestron	Std.Tail Rotor
without BVI	98 dB	134 dB
with BVI	102 dB	139 dB

shows, that the overall noise level is shifted in contrast to the measured values, but the increase due to the vortex interaction of 4 dB for the Fenestron and 5 dB for the standard tail rotor, is of the same amount as was found for the measurements.
For the calculated noise spectra the agreement

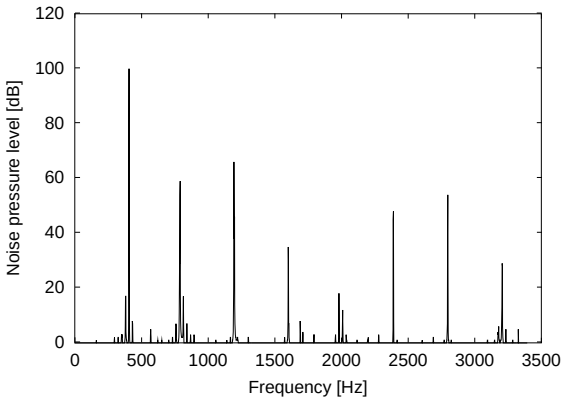

Figure 14: Spectrum of calculated noise of Fenestron with vortex interaction

with the measured spectra is not very satisfying. The amplitude of the fundamental frequency is too high and the decrease in magnitude per harmonic is to steep. This might result from some erroneous assumptions. So here some work still has to be done.

Conclusion

The influence of a Fenestron shroud on the interaction noise of the tail rotor blades interacting with the main rotor blade tip vortices during forward flight is investigated.. Due to the existence of a turbulent flow area inside the inner surface of the duct, the interaction point of the vortices is shifted to smaller radial positions for the Fenestron. So, the noise related to the frequency of the BVI is weak and only the Fenestron related frequencies are enforced. For the standard tail rotor without shroud, the vortices will interact at all radial positions, including the for the noise generation important area of the outer 20% of the rotor disc, and therefore the vortex related frequencies are of major importance. So, the shrouding of the tail rotor results in improved noise characteristics with respect to the blade vortex interaction. The emitted noise field is less annoying than that of a standard tail rotor.
The results of the theoretical examinations show good agreement regarding the increase of noise pressure levels due to BVI. But some refinement regarding the calculations of the noise spectra have to be done.

Acknowledgement

The authors like to thank the “**D**eutsche **F**orschungs **G**emeinschaft” DFG for funding this project over most of its duration.

References

[1] J. W. Leverton. Reduction of helicopter noise by use of a quiet tail rotor. *6th European Rotorcraft Forum*, Paper 24, 1980. Bristol.

[2] F. X. Caradonna, G. H. Laub, and C. Tung. An experimental investigation of the parallel blade-vortex interaction. *Workshop on Blade Vortex Ineractions*, 1984.

[3] C. Kitaplioglu, F. X. Caradonna, and C. L. Burley. Parallel blade-vortex interactions: An experimental study and comparison with computation. *American Helicopter Society Aeromechanics Specialists Conference*, 1995.

[4] G. R. Srinivasan, W. J. McCroskey, and J. D. Baeder. Aerodynamics of twodimensional blade-vortex interaction. *AIAA Journal*, 24(10):1569–1576, 1986.

[5] J. Shreier. *Experimentelle und theoretische Untersuchungen der Schallabstrahlung von Rotoren und Propellern, die sich in Wirbelfeldern bewegen*. Dissertation an der RWTH-Aachen, 1983.

[6] M. Heckl and H. A. Müller. *Taschenbuch der technischen Akustik*. Springer Verlag, 1994.

[7] C. N. Adkins and R. H. Liebeck. Design of optimum propellers. *Journal of Propulsion and Power*, 10(5):676–682, 1994.

[8] H. Schlichting and E. Truckenbrodt. *Aerodynamik des Flugzeugs*. Springer-Verlag, Berlin, 1960.

[9] M. J. Lighthill. On sound generated aerodynamically i. general theory. *Proceedings of the Royal Society of London*, 1107:564–587, 1952.

[10] J. E. Ffowcs Williams and D. L. Hawkings. Sound generation by turbulence and surfaces in arbitrary motion. *Philosophical Transactions Of The Royal Society Of London*, 264:321–342, 1969.

[11] F. Farassat. Linear acoustic formulas for calculation of rotating blade noise. *AIAA Journal*, 19(9):1122–1130, 1980.